Supplementary Material

for the article

Interplay mechanism of secondary phase particles and the extended dislocations in CdZnTe crystals

Yadong Xu[1, 2], Ningbo Jia[1], Yihui He[1], Rongrong Guo[1], Yaxu Gu[1], Wanqi Jie[1]

1. State Key Laboratory of Solidification Processing, Northwestern Polytechnical University, Xi'an 710072, China

2. Laboratory of Solid State Microstructures, Nanjing University, 210093, China

S1. Te-SP particles and dislocations in as-grown CZT crystals

As-grown CZT wafers from the same ingots were evaluated by IR transmission microscopy, as seen in Fig. S1(a). The resulting high-contrast IR images were obtained due to the strong IR absorption of Te, corresponding to its relatively narrow band gap (with the value of 0.33 eV [1]). In these images the distinct dark areas are associated with the presence of Te-rich SP particles in the CZT wafer. After etching by Everson solution, CZT $(111)_B$ surface was observed to give the grown-in dislocation density by counting the triangular pyramid etch pits, as shown in Fig. S1(b). By carefully controlling the cooling history to room temperature, dislocation clusters were not observed surrounding Te-rich SP particles.

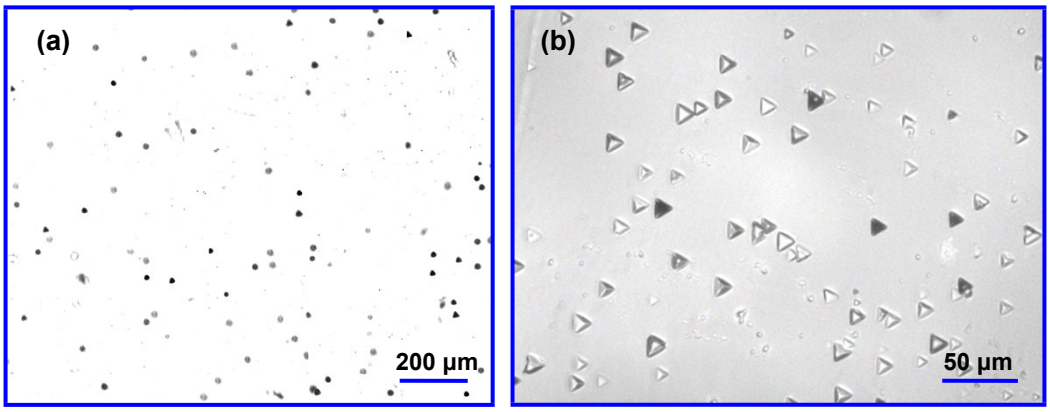

Fig. S1. (a) Typical IR images of Te-rich SP particles in as-grown CZT crystals, (b) Reflected-light image of the etch pits distribution on CZT $\{111\}_B$ face.

S2. IR transmission images

The distributions of Te inclusions in CZT samples have been investigated by transmission IR microscopy before and after the isothermal and thermal gradient annealing at metallic and Te overpressure, as shown in Fig. S2. The distinct dark spots showed up in the images represent the tellurium inclusions.

After isothermal annealing under Cd/Zn overpressure at 500°C, the density of

Te-rich SP particles is slightly lower, as seen the row of Ann-1 in Fig. S2. However, the average size of Te-SP is reduced from ~12.6 μm to ~10.3 μm.

The density of Te-rich SP particles is slightly lower than that in the as-grown CZT crystal, after isothermal annealing under Te overpressure, as seen the row of Ann-2 in Fig. S2. But the average size is enlarged, increases from ~14.5 μm to ~16.7 μm, which is possibly attributed to the large-size Te-SP ripening associated with the aggregation of the surrounding small-size Te inclusions or precipitates.

In respect of the temperature-gradient annealing under metallic overpressure, large-size Te SP particles are significantly eliminated after annealing, only small dark dots with size of 5-10 μm present, as seen the row of Ann-3 in Fig. S2.

The temperature-gradient annealing under Te overpressure was utilized at 650/750°C (CZT/Te). However, tellurium sources are inclined to deposit on CZT surface after annealing. Surface layer of ~0.1 mm is removed prior to do IR image, it is suggest that both size and density of Te-SP particles reduce, as seen the row of Ann-4 in Fig. S2.

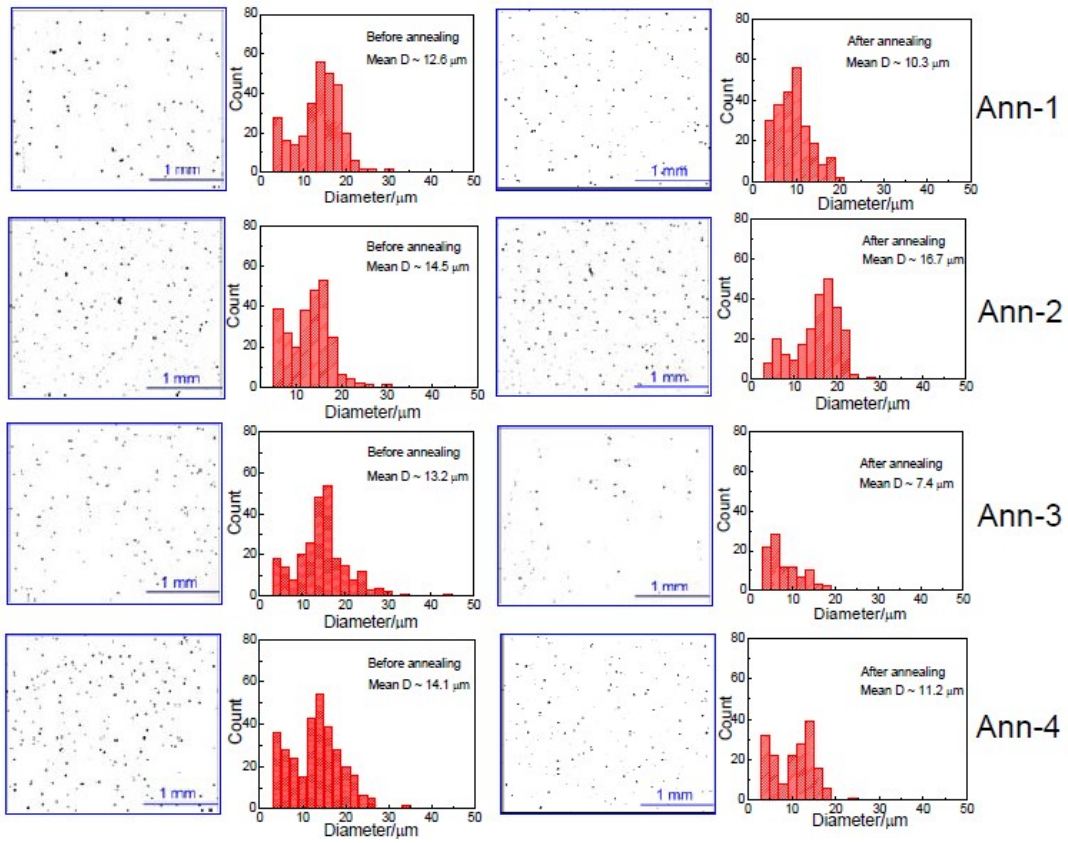

Fig. S2. Typical IR images and the size distributions of Te-rich SP particles before and after annealing.

S3. Comparison between Cathodoluminescence (CL) image and the corresponding SEM image

Owing to the low luminescence efficiency of CZT, the sample has to be cooled to ~80 K to ensure the good contrast of image. Typical panchromatic CL micrograph (700-900 nm) of a Te inclusion embedded on $\{111\}_B$ at 80 K and the SEM image of the same region are shown in Fig. S3. The dark dots in the panchromatic CL image associated with Te_i-related defects were suggested to be responsible for the non-radiative recombination process at the dislocation-rich region [2]. The dark dots line up with a cross in the blue dash dotted circles is different from the distribution in the red dash dotted circles, as seen in Fig. S3(a). According to the same region after selective-etching shown in Fig. S3(b), it was ascertained that the non-radiative centers enrichment was determined by the special dislocations pattern, which associated with the dislocations slip systems.

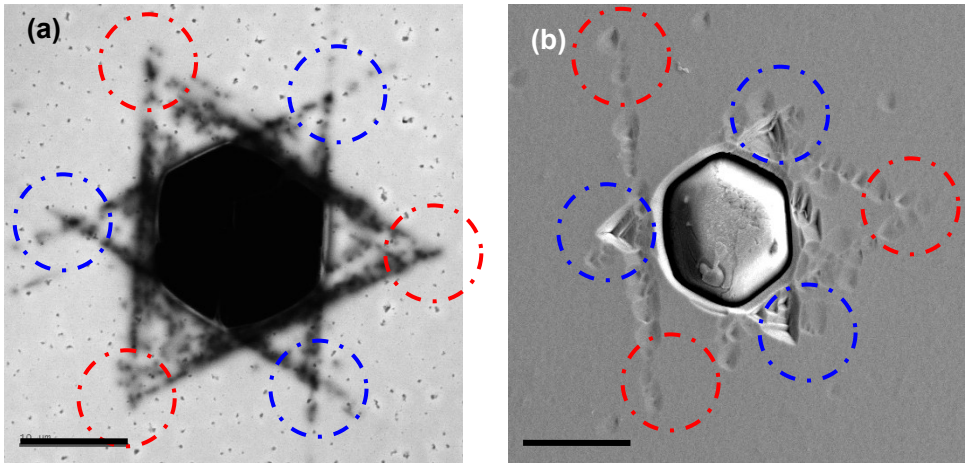

Fig. S3. (a) Typical panchromatic CL micrograph (700-900 nm) of a Te inclusion embedded on $\{111\}_B$ at 80 K. (b) SEM image of the same region after selective-etching. All scale bars correspond to 10 μm.

S4. Te-SP and dislocation etch pits after isothermal annealing under Te overpressure

In the case of isothermal annealing under Te overpressure, dislocations and Te-SP are observed on $\{111\}_B$ face after defect-selective etching, as shown in Fig. S4. Triangular pyramid etch pits distribute randomly with a flat bottom cavity formed by the separation of Te-SP. In Fig. S4(b) and (c), the dark and grey triangular dots represent Te-SP and dislocation etch pits, respectively. Clearly, neither 'radial-shaped' nor 'star-shaped' dislocations clusters appears.

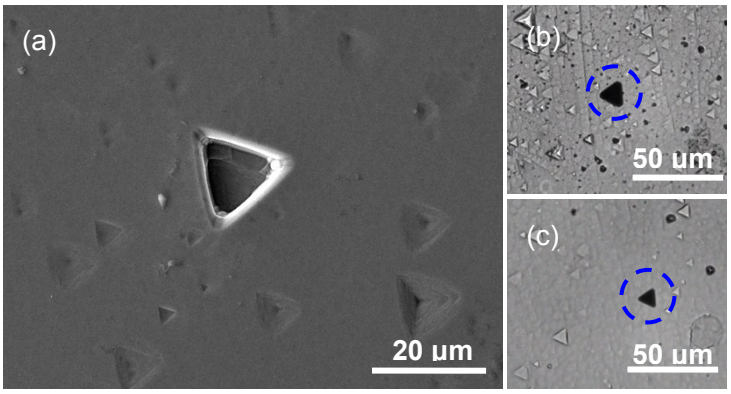

Fig. S4. (a) SEM images of CZT $\{111\}_B$ surface after etching, with Te-SP separated. (b) and (c) are the typical IR images of the etch pits and Te-SP.

S5. FIB processing and TEM results

Focused ion beam/scanning electron microscope (FIB/SEM) was used to prepare thin sections for transmission electron microscopy (TEM) studies, as shown in Fig. S5. Low-energy ion-beam milling was employed to improve sample quality by reducing the thickness of the damaged layer. The phase structure and lattice deformation of local areas were identified by HRTEM as seen in Fig. S6. The coherent and incoherent precipitates surrounding Te-SP were observed by revealing a cross-sectional view, which reflects the Ostwald ripening of Te-SP during isothermal annealing under Te overpressure, more details in [3].

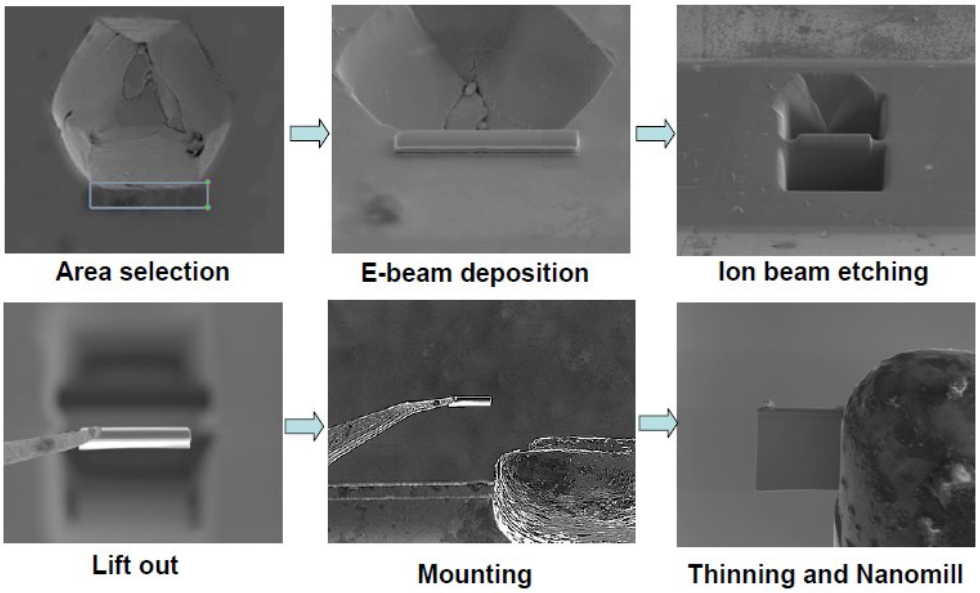

Fig. S5. The entire preparation processes for the thin section by FIB/SEM.

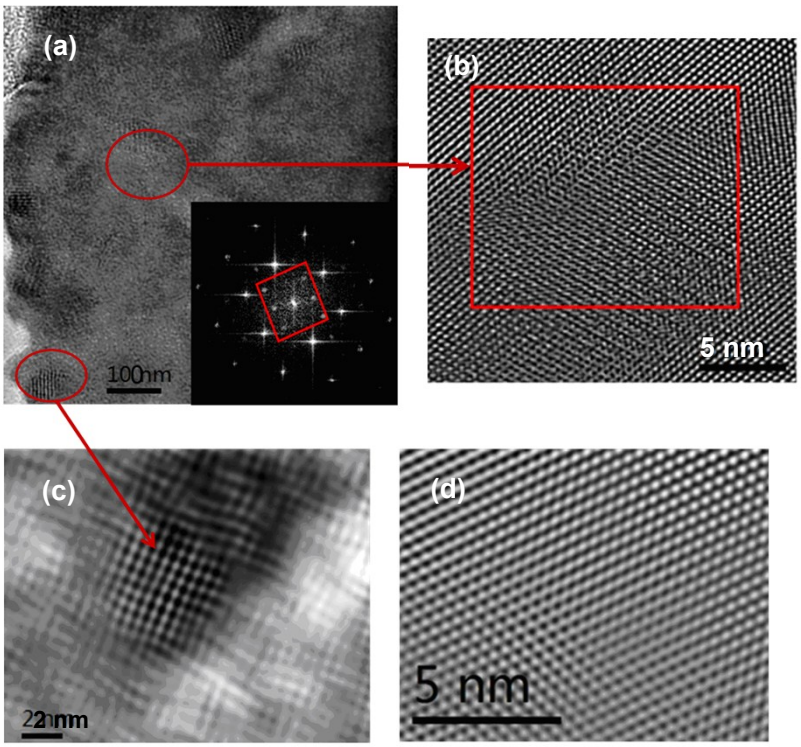

Fig. S6. (a) TEM images of the local area surrounding Te-SP. Insert is the FFT image corresponding to the stripe region. (b) Enlarged coherent precipitate. (c) Enlarged incoherent precipitate. (d) Enlarged CZT matrix lattice.

Reference

[1] H. N. Jayatirtha, D. O. Henderson, A. Burger, M. P. Volz, *Appl. Phys. Lett*. 1993, **62**, 573-575.

[2] Y. He, W. Jie, Y. Xu, Y. Wang, Y. Zhou, H. Liu, T. Wang, G. Zha, *Scripta Materialia*. 2014 **82**, 17-20.

[3] Y. He, Y. Xu, J. Jia, R. Guo, Y.Gu, Y. Wang, W. Jie, Submited to Acta Materials, 2015.